Ablation of *mpeg*$^{+}$ Macrophages Exacerbates *mfrp*-Related Hyperopia

Zachary J. Brandt,[1] Ross F. Collery,[2] Joseph C. Besharse,[2] and Brian A. Link[1]

[1]Department of Cell Biology, Neurobiology and Anatomy, Medical College of Wisconsin, Milwaukee, Wisconsin, United States
[2]Department of Ophthalmology and Visual Sciences, Medical College of Wisconsin, Milwaukee, Wisconsin, United States

Correspondence: Brian A. Link, Department of Cell Biology, Neurobiology and Anatomy, Medical College of Wisconsin, 8701 Watertown Plank Road, Milwaukee, WI 53226, USA; blink@mcw.edu.

Received: May 3, 2021
Accepted: September 8, 2021
Published: December 16, 2021

Citation: Brandt ZJ, Collery RF, Besharse JC, Link BA. Ablation of *mpeg*$^{+}$ macrophages exacerbates *mfrp*-related hyperopia. *Invest Ophthalmol Vis Sci.* 2021;62(15):13. https://doi.org/10.1167/iovs.62.15.13

Purpose. Proper refractive development of the eye, termed emmetropization, is critical for focused vision and is impacted by both genetic determinants and several visual environment factors. Improper emmetropization caused by genetic variants can lead to congenital hyperopia, which is characterized by small eyes and relatively short ocular axial length. To date, variants in only four genes have been firmly associated with human hyperopia, one of which is *MFRP*. Zebrafish *mfrp* mutants also have hyperopia and, similar to reports in mice, exhibit increased macrophage recruitment to the retina. The goal of this research was to examine the effects of macrophage ablation on emmetropization and *mfrp*-related hyperopia.

Methods. We utilized a chemically inducible, cell-specific ablation system to deplete macrophages in both wild-type and *mfrp* mutant zebrafish. Spectral-domain optical coherence tomography was then used to measure components of the eye and determine relative refractive state. Histology, immunohistochemistry, and transmission electron microscopy were used to further study the eyes.

Results. Although macrophage ablation does not cause significant changes to the relative refractive state of wild-type zebrafish, macrophage ablation in *mfrp* mutants significantly exacerbates their hyperopic phenotype, resulting in a relative refractive error 1.3 times higher than that of non-ablated *mfrp* siblings.

Conclusions. Genetic inactivation of *mfrp* leads to hyperopia, as well as abnormal accumulation of macrophages in the retina. Ablation of the mpeg1-positive macrophage population exacerbates the hyperopia, suggesting that macrophages may be recruited in an effort help preserve emmetropization and ameliorate hyperopia.

Keywords: *MFRP*, macrophages, zebrafish, hyperopia

Emmetropization is the precise regulation of size, morphology, and relative proportions of ocular tissues and is critical for proper refraction of light and thus clear vision. Improper emmetropization results in either myopia or hyperopia. Myopia is caused by a relative elongation of the axial length and is the more common and better studied refractive error. Hyperopia most often occurs when the axial length is too short for the focusing apparatus of the eye, resulting in light focusing behind the retina. Comparatively less is known regarding the mechanisms of hyperopia.

Although variants in many genomic regions are associated with changes in refractive error, variants in just a few genes have been associated with monogenic high hyperopia or nanophthalmos.[1–4] Homozygous or compound heterozygous mutations of *MFRP*, which encodes membrane-type frizzled-related (MFRP) protein, are associated with microphthalmia, high hyperopia, foveoschisis, areas of retinal pigmented epithelium (RPE) atrophy, and optic disc drusen in humans.[1,2,5–11] Evidence for the conservation of *MFRP* function comes from multiple animal models. First, two mouse models of spontaneous retinal degeneration, *rd6* and *rdx*, have identified mutations in *Mfrp* as their cause.[12,13] Although these mutations resulted in retinal degeneration, initial analysis of homozygous mutants did not find hyperopia. However, examination of the *rd6* model using non-invasive imaging found that these mice indeed have slight decreases in axial length and that this effect could be rescued by gene therapy.[14,15] Our lab utilized zebrafish to investigate the effects of *mfrp* mutation. In contrast to mice, zebrafish homozygous for *mfrp* mutations do not develop retinal degeneration but do recapitulate the pronounced hyperopia seen in humans homozygous for *MFRP* alterations.[16] These findings illustrate the role of Mfrp in proper emmetropization and its functional conservation across multiple species.

Although both mouse and zebrafish models display hyperopic phenotypes in the absence of Mfrp, neither model fully recapitulates the full spectrum of human *MFRP*-related phenotypes, as mice appear to exhibit only small changes in eye size, failing to develop high hyperopia, and zebrafish mutants do not present photoreceptor degeneration. Intriguingly disruption of *mfrp* in both zebrafish and mice causes accumulation of subretinal macrophages.[12,16,17]

Accumulation of retinal macrophages may also occur in human *MFRP*-related pathology. The presence of round yellow-white flecks has been documented in patients with *MFRP*-associated microphthalmia.[18] Under fundus microscopy the subretinal macrophages present in the *Mfrp* mouse models also share this white fleck appearance.[12] These observations suggest that accumulation of retinal macrophages is a unified feature of *Mfrp* mutations across species.

Based on the accumulation of macrophages seen in two distinct animal models of MFRP-related hyperopia, we hypothesized that those retinal macrophages, or macrophages within the eye in general, may function to regulate emmetropization. In order to test this hypothesis, we utilized established cell-specific ablation techniques in the zebrafish model. We found that, although ablation of macrophages in wild-type (WT) fish does not affect basal emmetropization, deletion of this population exacerbates the hyperopia observed in *mfrp* mutant fish. We also investigated changes in proliferation, cell death, and scleral collagen fiber morphology of *mfrp* mutant zebrafish.

Methods

Histology and Transmission Electron Microscopy

Eyes were fixed with 1.0% paraformaldehyde, 2.5% glutaraldehyde, and 3.0% sucrose in 0.06-M cacodylate buffer overnight at 4°C. Samples were then washed in cacodylate buffer and post-fixed with 1% osmium tetroxide and then dehydrated by a series of methanol washes. Larvae were infused with Epon 812 resin (Electron Microscopy Sciences, Hatfield, PA, USA) through two 15-minute acetonitrile washes followed by 1:1 acetonitrile:Epon incubation for 1 hour, and 100% Epon incubation overnight. Finally, larvae were embedded in 100% Epon and hardened at 65°C for 24 hours. Then, 1-µm transverse serial sections through the length of the larvae were cut via microtome and stained with Toluidine Blue for light microscopy. Light microscopy images were taken using a NanoZoomer 2.0-HT (Hamamatsu Photonics K.K., Hamamatsu City, Japan). For transmission electron microscopy (TEM) analysis, 70-nm sections were cut, collected on hexagonal grids, and stained with uranyl acetate and lead citrate, followed by imaging on a Hitachi H-600 Transmission Electron Microscope (Hitachi, Ltd., Tokyo, Japan).

Paraffin Histology

Eyes utilized for paraffin histology were immersed in 4% paraformaldehyde overnight at 4°C and embedded in paraffin blocks for sectioning. Then, 4-µm sections were obtained and stained with hematoxylin and eosin for analysis, with serial unstained sections used for immunofluorescent staining. Unstained sections underwent de-paraffinization with xylenes and an ethanol gradient prior to heated antigen retrieval in antigen retrieval solution (Dako; Agilent Technologies, Santa Clara, CA, USA). Immunofluorescent staining was then performed as follows.

Retina Flat-Mount Preparation

Retina flat-mount immunofluorescent staining was performed on dissected eyecups that were fixed overnight at 4°C in 4% paraformaldehyde. Before staining, the lens, cornea, and anterior chamber of the eye were dissected away to allow better access to the tissue. Retinae were washed in phosphate-buffered saline (PBS) to remove fixative. An identifying notch was cut into the dorsal side of the retina to maintain proper anatomical positioning. Four roughly equidistant cuts were made from the outside of the retina toward the middle in order to relieve tension and flatten the globe under a coverslip. Immunofluorescent staining was then performed as follows.

Immunofluorescence

For both paraffin sections and retina flat-mount preparations, standard immunostaining followed with 1-hour incubation in blocking solution (2% normal goat serum, 1% Triton X-100, and 1% Tween 20 in PBS). Larvae were incubated in primary antibodies overnight in blocking solution at room temperature or 4°C. Embryos were then washed three times for 1 hour in 1% Tween 20 in PBS. Antibody detection was performed using Invitrogen Alexa Fluor 488 and 568 conjugated secondary antibodies (Thermo Fisher Scientific, Waltham, MA, USA) at 1:800 dilution in blocking solution overnight at 4°C followed by washes with 1% Tween 20 in PBS. The following primary antibodies and concentrations were utilized:

- 1:200 mouse anti-4C4 (gift from Peter Hitchcock, University of Michigan)
- 1:500 rabbit anti-lymphocyte cytosolic protein 1 (Lcp1, L-plastin; GTX124420; GeneTex, Irvine, CA, USA)
- 1:500 mouse anti-green fluorescent protein (GFP; JL-8; Takara Bio, Shiga, Japan)
- 1:500 ABfinity rabbit anti-GFP (G10362; Thermo Fisher Scientific)

Spectral Domain–Optical Coherence Tomography

Zebrafish eyes were imaged using an Envisu R2200 spectral-domain optical coherence tomography (SD-OCT) imaging system with a 12-mm telecentric lens (Bioptigen, Morrisville, NC, USA) using a Broadlighter T870 light source centered at 878.4 nm with a 186.3-nm band width (Superlum Diodes, Cork, Ireland). Axial length, lens diameter, and retinal radius were measured for populations of zebrafish at 56 days post-fertilization (dpf), as described previously.[19] Both eyes were measured for each fish. In statistical analysis, only the right eye was utilized.

Eye and Body Length Measurement

The following zebrafish eye dimensions were measured: axial length (front of cornea to back of RPE), lens diameter (anterior surface of lens to posterior surface), and retinal radius (center of lens to the back of the RPE). Body length was measured from the tip of the head to the end of the trunk (before the caudal fin). Relative refractive error was calculated as 1 – (retinal radius/F), where idealized focal length F= lens radius × 2.324, using a coefficient extrapolated from a large population group (n= 240) plot of lens radius versus retinal radius.[19] Relative refractive error values are unitless, with values lower than zero indicating that the eye is myopic (or that the observed distance from lens center to RPE is greater than the expected retinal radius) and values greater than zero indicating that the eye is hyperopic (or that

Investigative Ophthalmology & Visual Science

the observed distance from lens center to RPE is less than the expected retinal radius). The relative refractive error is based on the following assumptions: (1) the refractive index of the fish lens is constant, and (2) the distance from the center of the lens to the RPE is equal to the focal length of the lens of WT fish.

Metronidazole Treatment

All fish used for macrophage ablation experiments were raised under normal conditions from 0 to 14 dpf. On 14 dpf, fish were randomly separated into control and experimental groups. Experimental groups were reared in stationary tanks with 7-mM metronidazole (MTZ; M3761-100G; Sigma-Aldrich, St. Louis, MO, USA) dissolved in fish facility water from 6:00 PM to 9:00 AM daily. From 9:00 AM to 6:00 PM, fish were returned to the circulating facility water in 3-L tanks for rearing and feeding. From 14 dpf to 21 dpf, fish in the experimental group were kept in 500 mL of MTZ for treatments, and 21-dpf and older fish were kept in 1 L of MTZ for treatments. It is important to note that fresh MTZ treatments occurred daily until the final time point. This consistent treatment was aimed at achieving consistent depletion of the targeted cell population from 14 dpf until 56 dpf. Untreated control groups were also moved to stationary tanks with equivalent volumes of water during MTZ treatments.

Collagen Hybridizing Peptide Staining

For collagen hybridizing peptide (CHP) staining, paraffin sections were used, and standard de-paraffinization with xylenes and an ethanol gradient were performed. Importantly, no antigen retrieval steps were taken in order to avoid denaturing or unfolding of collagenous proteins in the samples. Samples were then blocked in 5% goat serum for 20 minutes at room temperature. To stain the sample, a 20-mM CHP–Cy3 conjugate (60520; Echelon Biosciences, Salt Lake City, UT, USA) working solution diluted in PBS was used. Prior to staining, the working solution was heated at 80°C for 5 minutes and then rapidly brought to room temperature by placing it on ice for 30 seconds. The working solution was then quickly added to slides outlined with a PAP pen (Abcam, Cambridge, UK) and incubated overnight at 4°C. Counterstaining with 4′,6-diamidino-2-phenylindole (DAPI) followed prior to imaging.

Zebrafish

All transgenic and mutant lines were generated and maintained in the ZDR genetic background originally purchased from Aquatica Biotech, Sun City Center, Florida. WT siblings or cousins were used as control groups. All animal experiments were approved by the Institutional Animal Care and Use Committee of the Medical College of Wisconsin.

Transgenic Lines and Mutant Lines

Tg(*mpeg1*:NTR-eyfp) is a transgenic line that utilizes an isolated 1.86-kb sequence of the promoter region of macrophage expressed gene 1 (*mpeg1*) identified by Ellett et al.[20] to drive expression of an enhanced yellow fluorescent protein (eYFP)-tagged, human codon-optimized version of the *Echerichia coli* enzyme nitroreductase. This line has previously been used in conjunction with MTZ treatment for both short- and long-term ablation of macrophages.[20–22]

mfrp^{MW78} is a mutant line that contains a 5-bp deletion in exon 8 of zebrafish *mfrp* and is predicted to change the reading frame of Mfrp protein causing premature truncation. Mfrp immunostaining on cryosections previously indicated a loss of protein detection by an Mfrp-specific antibody, supporting the notion that this mutation leads to complete loss of Mfrp function.[16]

Results

To address the role of macrophages in emmetropization, we sought to deplete the macrophage population during ocular growth and assess potential changes in axial length and refractive error. We chose zebrafish as our model organism because they display a larger shift in refractive state upon *mfrp* deletion than the *Mfrp* mutant mouse models, allowing for easier detection of phenotypic change.[15,16] For efficient macrophage ablation we used an established chemical–genetic system.[23] Using macrophage promoter *mpeg1*[20] we expressed bacterial nitroreductase (NTR) fused to eYFP specifically in macrophages. Fish carrying this transgene are termed *mpeg1:*NTR-eYFP^{+}.[21] On its own, NTR expression does not harm cells; however, it converts the nontoxic prodrug MTZ into a cytotoxic metabolite that results in autonomous DNA crosslinking and subsequent cell death. This system has been effectively utilized for the ablation of multiple cell types in zebrafish.[23]

Ablation of Macrophages in WT Zebrafish Did Not Significantly Impact Emmetropization

To determine the best temporal strategy for macrophage depletion we had previously observed ocular growth of WT and *mfrp*$^{-/-}$ fish over time by SD-OCT.[16] In both populations, we found that 15 to 84 dpf encompassed the highest growth rates in ocular anatomy, as well as overall body size.[16] Prior to 31 dpf, no differences in ocular biometry or relative refractive error were seen between WT and *mfrp*$^{-/-}$ eyes; at 31 dpf and following, *mfrp*$^{-/-}$ eyes begin to show significant decreases in axial length, lens diameter, retinal radius, and body length relative to WT fish.[16] By 31 dpf, WT eyes reach a stable relative refractive error measurement that continued through at least 149 dpf.[16] In contrast, at 31 dpf, *mfrp*$^{-/-}$ eyes exhibited slightly higher relative refractive error, and this difference was accentuated at 84 dpf, when the magnitude of difference between WT and *mfrp* relative refractive error appears to level off.[16] Given this information, we chose to ablate macrophages starting at 14 dpf and continuing through 56 dpf. After 14 dpf, treatment was chosen to allow for the normal development and organization of the retina, avoiding potential adverse effects of macrophage ablation on early development and focusing solely on ocular growth as it pertains to eye size and refractive state. We chose 56 dpf as the endpoint because it represents a time when WT eyes have reached an equilibrium regarding relative refractive error, but it is also a period when active emmetropization must still occur given that the absolute size of the eye continues to grow and that pathologic *mfrp*$^{-/-}$ eyes exhibit significantly higher relative refractive error at this time.

To examine the effects of *mpeg1*$^{+}$ cell ablation on emmetropization, we allowed *mpeg1:*NTR-eYFP^{+} fish and their non-transgenic WT cousins to grow to 8 weeks of age, or more precisely 56 dpf, with or without MTZ treatment. MTZ was administered through daily bath applications

Investigative Ophthalmology & Visual Science

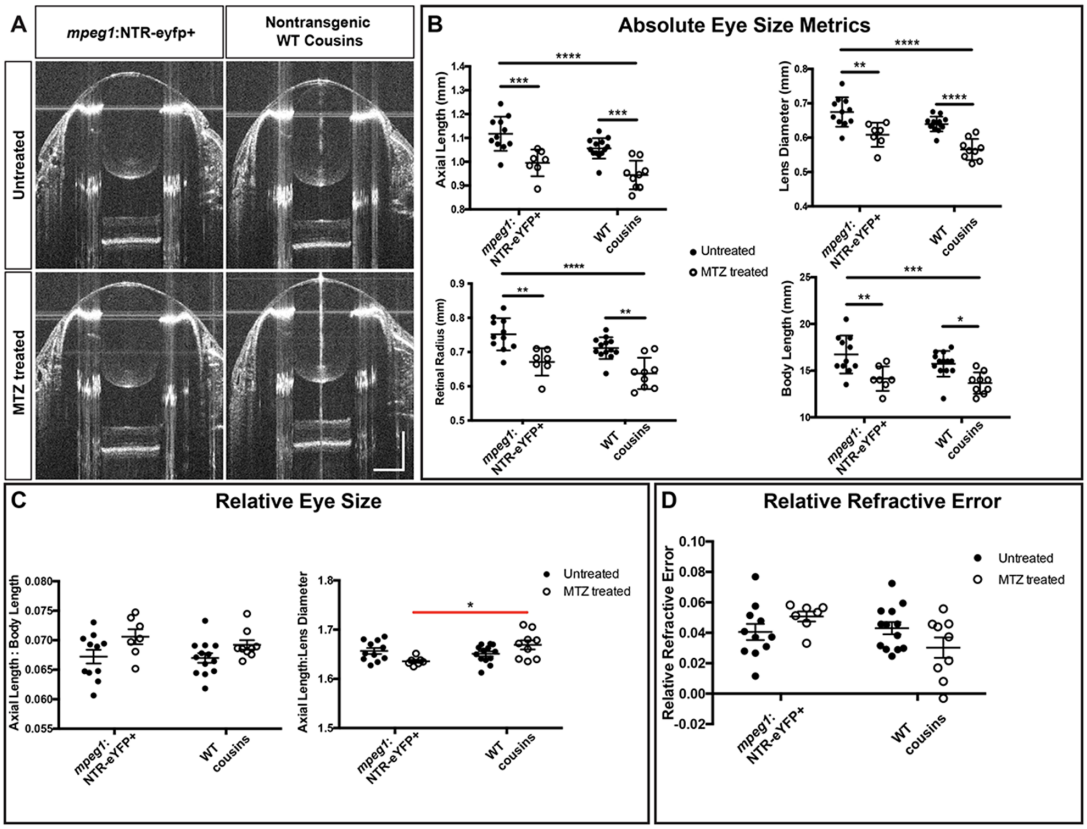

Figure 1. Ablation of macrophages in WT zebrafish did not significantly impact emmetropization. (**A**) Representative SD-OCT B-scans from the center of *mpeg1:*NTR-eYFP^{+} eyes and their WT cousins with or without MTZ treatment. (**B**) Axial length, lens diameter, retinal radius, and body length of *mpeg1:*NTR-eYFP^{+} fish and their WT cousins with or without MTZ treatment. (**C**) Axial length normalized to body length and lens diameter. (**D**) Relative refractive error. Two-way ANOVA was used for statistical analysis for (**B**) to (**D**). *P* values are shown from Tukey's multiple comparisons for post hoc analysis. *Red bars* indicate statistical significance likely due to *mpeg1*$^{+}$ cell ablation. $^{*}P < 0.05$, $^{**}P < 0.01$, $^{***}P < 0.001$, $^{****}P < 0.0001$. For *mpeg1:*NTR-eYFP^{+} untreated, $n = 11$; for *mpeg1:*NTR-eYFP^{+} MTZ treated, $n = 7$; for WT cousins untreated, $n = 13$; for WT cousins MTZ treated, $n = 9$.

starting at 14 dpf. Fresh MTZ was administered every day from 14 dpf to 56 dpf with the aim of achieving constant *mpeg1*$^{+}$ cell ablation throughout that time. Efficient ablation of macrophages in transgenic fish was confirmed by imaging eYFP-expressing cells in retinal flat-mount preparations, resulting in near complete depletion (Supplementary Fig. S1A-A"). When fish reached 56 dpf they were anesthetized and imaged via SD-OCT to measure axial length, lens diameter, and retinal radius (Figs. 1A, 1B), which were used to calculate refractive error as described previously (see Methods).[19]

To properly assess changes in eye size as it relates to refractive error, it is important to understand how axial length was normalized. We normalized the axial length of the eye using two separate parameters, lens diameter and body length. Normalizing to lens diameter allowed us to test whether an individual eye was the correct length to match the focusing power of the eye, as the lens contributes the majority of the refractive power of the zebrafish eye.[19] Alternatively, normalizing to body length allowed us to assess whether an eye was considered large or small relative to overall body size without revealing anything about the refractive properties of the eye. We have previously shown that both of these measurements correlate linearly with axial length in WT fish under normal growth conditions.[19]

MTZ treatment resulted in overall smaller zebrafish, as measured by decreases in axial length, lens diameter, retinal radius, and body length (Fig. 1B). This was true in both the presence and absence of *mpeg1:*NTR-eYFP expression, suggesting that MTZ treatment causes developmental delay or slower overall body growth independent of cell-specific ablation. After normalization to body length, no changes in axial length were detectable (Fig. 1C). We also normalized to lens diameter, and, although *mpeg1*:NTR-eYFP^{+} MTZ-treated eyes had significantly shorter ratios of axial length to lens diameter than their non-transgenic, MTZ-treated cousins, neither MTZ-treated group had significant changes relative to their untreated siblings (Fig. 1C). To more specifically assess the refractive state of these eyes, we calculated relative refractive error as described previously.[19] No significant differences in relative refractive error were observed (Fig. 1D). Taken together, these results suggest that *mpeg*$^{+}$ macrophage ablation does not significantly alter emmetropization in WT zebrafish.

Macrophage Ablation in *mfrp* Mutants

Although macrophage ablation did not significantly alter the relative refractive error of WT zebrafish, the previously documented macrophage accumulation in *mfrp* mutants led us to hypothesize that they may still play a role in modulating the

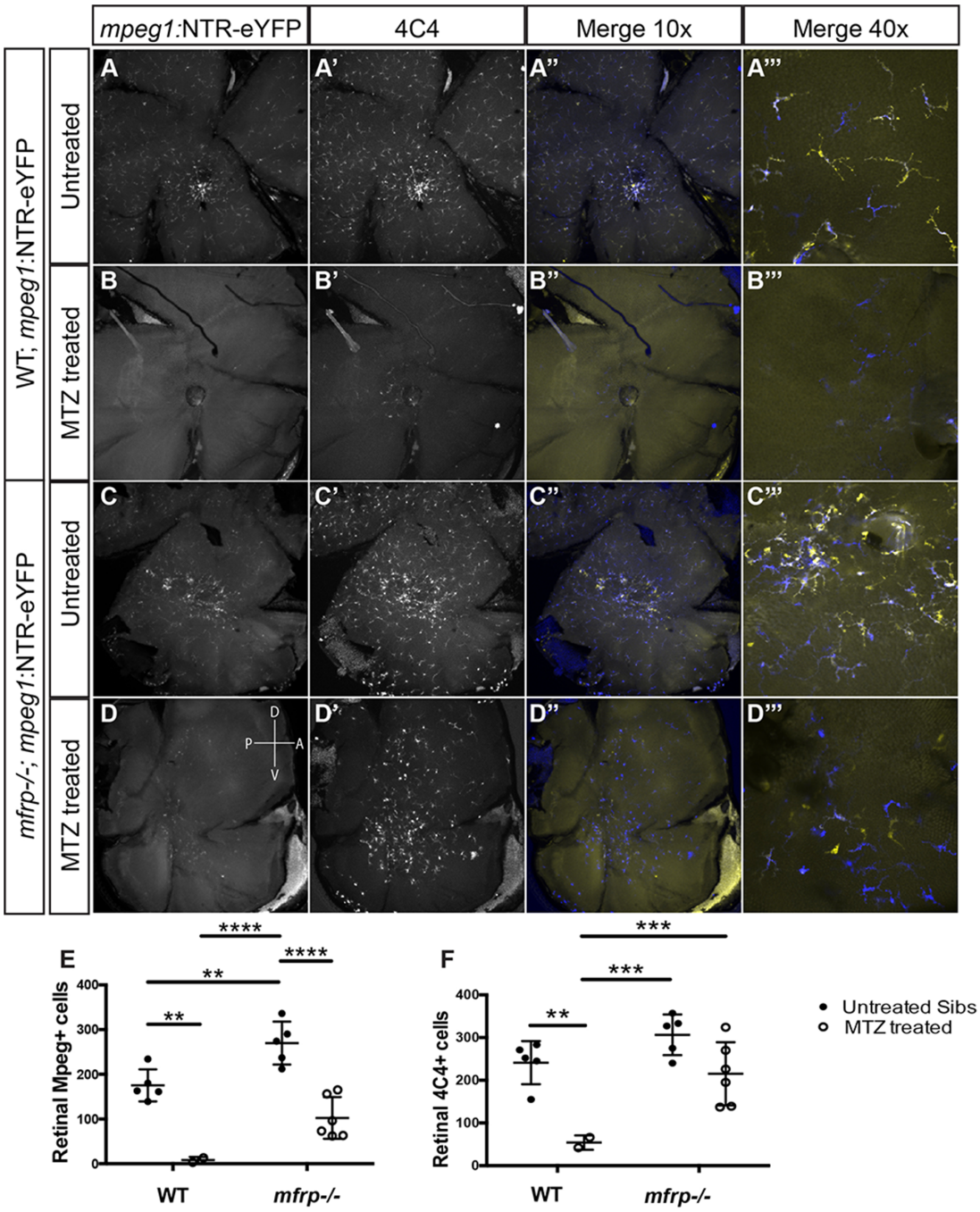

Figure 2. Efficient macrophage ablation in the *mfrp* retina. (**A–D**) *mpeg1:*NTR-eYFP expression in WT and *mfrp*$^{-/-}$ retina flat-mount preparations with and without MTZ treatment. (**A'-D'**) Immune staining for 4C4 antibody marking macrophages. (**A"–D"**) Merged and colorized images of **A–D'**, with *blue* representing 4C4 and *yellow* representing YFP. (**A'"–D'"**) Higher magnification images of (**A"**) to (**D"**). (**E**, **F**) Cell counts of *mpeg1:*NTR-eYFP^{+} cells (**E**) or 4C4^{+} cells (**F**) in WT and *mfrp*$^{-/-}$ retina flat-mount preparations with and without MTZ treatment. Two-way ANOVA was used for statistical analysis. Sidak's multiple comparisons were used for post hoc analysis. $^{*}P < 0.05$, $^{**}P < 0.01$, $^{***}P < 0.001$, $^{****}P < 0.0001$. For WT untreated, $n = 5$; for WT MTZ treated, $n = 2$; for *mfrp*$^{-/-}$ untreated, $n = 5$; for *mfrp*$^{-/-}$ MTZ treated, $n = 6$.

pathologic hyperopic state. To evaluate this, we employed the same macrophage ablation strategy on *mfrp* mutant and heterozygous siblings. Again, highly efficient ablation of WT macrophages was observed by *mpeg1:*NTR-eYFP expression, as well as using the 4C4 antibody, which labels macrophages and microglial cells in zebrafish (Figs. 2A–2B"', 2E, 2F).[24] Although nearly all transgene expressing cells were depleted, some 4C4^{+} cells escaped ablation, likely due to incomplete overlap in expression of the 4C4 antigen and *mpeg1* transgene. As expected, *mfrp* mutant fish showed significant increases in *mpeg1:*NTR-eYFP^{+} cells, with focal increases at the central retina (Figs. 2C–2C"'). In *mfrp*$^{-/-}$

Investigative Ophthalmology & Visual Science

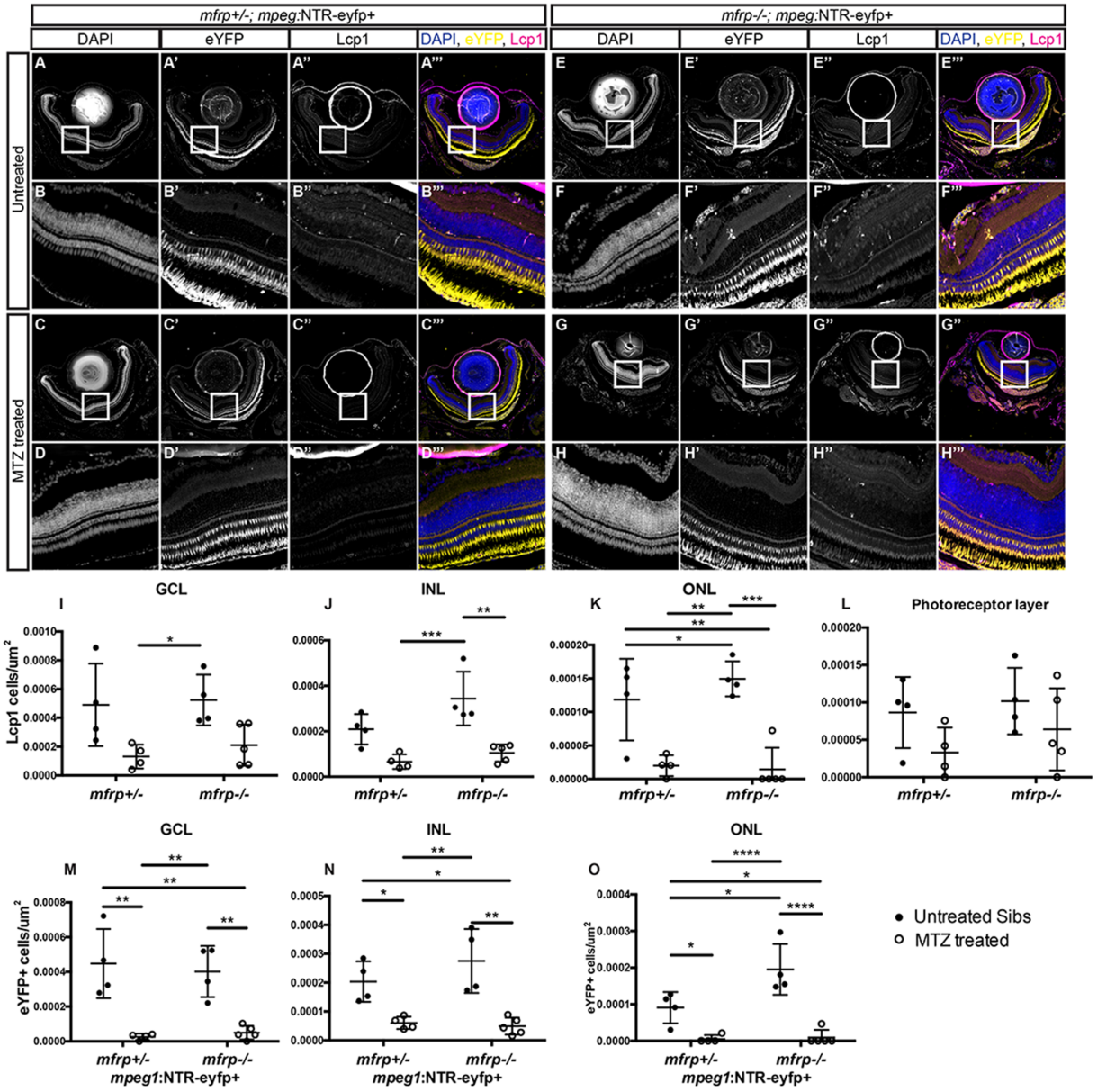

Figure 3. Distribution of macrophage accumulation and ablation across *mfrp*$^{+/-}$; and *mfrp*$^{-/-}$ retinae. (**A–H**) Representative images of central retina sections from *mfrp*$^{+/-}$; *mpeg1:*NTR-eYFP^{+} and *mfrp*$^{-/-}$; *mpeg1:*NTR-eYFP^{+} MTZ treated and untreated fish. (**A–H**) Grayscale DAPI images at low magnification (**A**, **C**, **E**, **G**) and high magnification (**B**, **D**, **F**, **H**). (**A'–H'**) Grayscale eYFP images at low magnification (**A'**, **C'**, **E'**, **G'**) and high magnification (**B'**, **D'**, **F'**, **H'**). (**A"–H"**) Grayscale Lcp1 images at low magnification (**A"**, **C"**, **E"**, **G"**) and high magnification (**B"**, **D"**, **F"**, **H"**). Colorized merged images with DAPI are shown in *blue*, eYFP in *yellow*, and Lcp1 in *magenta*; images are at low magnification (**A'"**, **C'"**, **E'"**, **G'"**) and high magnification (**B'"**, **D'"**, **F'"**, **H'"**). (**I–L**) Quantification of the number of Lcp1^{+} cells per μm^2 in the ganglion cell layer (**I**) and inner (**J**) and outer (**K**) nuclear layer, and photoreceptor layer (**L**). (**M–O**) Quantification of the number of eYFP^{+} cells per μm^2 in the ganglion cell layer (**M**) and inner (**N**) and outer (**O**) nuclear layer. *Error bars* represent standard deviations. Two-way ANOVA was used for statistical analysis for (**I**) to (**O**). *P* values are shown from Tukey's multiple comparisons for post hoc analysis. $^{*}P < 0.05$, $^{**}P < 0.01$, $^{***}P < 0.001$, $^{****}P < 0.0001$. For *mfrp*$^{+/-}$ untreated, $n = 4$; for *mfrp*$^{+/-}$ MTZ treated, $n = 4$; for *mfrp*$^{-/-}$ untreated, $n = 4$; for *mfr*$^{-/-}$ MTZ treated, $n = 5$.

fish, we saw depletion of *mpeg1:*NTR-eYFP–expressing cells; however, the effect was not as complete as in WT fish (Figs. 2C–2E). The 4C4 cell counts were not significantly decreased (Figs. 2C', 2D', 2F). Although the ablation of our *mpeg1:*NTR-eYFP–expressing cells remained efficient and significant, these results reveal that some macrophages that accumulate in *mfrp*$^{-/-}$ eyes remained.

To obtain more detailed spatial information regarding the macrophage accumulation in *mfrp* mutants, as well as their ablation, we performed immunofluorescent staining on histological sections. We labeled eYFP^{+} cells using a GFP antibody and co-stained for Lcp1 as an additional macrophage marker.[25] Nuclei were stained with DAPI to identify the retinal layers. In *mfrp*$^{+/-}$; *mpeg1:*NTR-eyfp^{+} untreated control fish, eYFP^{+} cells were seen sporadically across all layers of the retina. The ganglion cell layer and inner nuclear layer (INL) contained the highest frequency of these cells, but eYFP^{+} cells would also be found in the outer

nuclear layer (ONL). In control fish, nearly all eYFP$^+$ cells observed were also Lcp1$^+$ (Figs. 3A–3B"', 3I–3K, 3M–3O). The strong endogenous fluorescence within the photoreceptor layer precluded accurate quantitation of eYFP$^+$ cells in this layer; however, Lcp1 staining showed small numbers of macrophages present there, as well (Fig. 3L). MTZ treatment efficiently reduced or completely depleted eYFP$^+$ cells across all layers of *mfrp*$^{+/-}$; *mpeg1:*NTR-eyfp$^+$ eyes (Figs. 3C–3D"', 3M–3O). Though seemingly reduced, sporadic Lcp1$^+$ cells remained at slightly higher levels than eYFP$^+$ cells, revealing that some macrophages escaped ablation. In *mfrp*$^{-/-}$; *mpeg1:*NTR-eyfp$^+$ untreated eyes, both eYFP$^+$ and Lcp1$^+$ cells were noted across all layers of the retina (Figs. 3E–3F"'). However, statistical analysis showed a significant increase in the frequency of both eYFP$^+$ and Lcp1$^+$ cells only in the ONL (Figs. 3K, 3O). MTZ treatment was similarly effective in *mfrp*$^{-/-}$; *mpeg1:*NTR-eyfp$^+$ fish, as eYFP$^+$ cells were greatly reduced or completely depleted across all layers of the retina (Fig. 3M–3O). Lcp1$^+$ cells were also decreased in the INL and ONL (Figs. 3J, 3K). These data highlight the efficient ablation of macrophages across all layers of the eye and identify the ONL as the specific location of increased macrophage presence in *mfrp*$^{-/-}$ fish.

Macrophage Ablation Exacerbated Hyperopia in *mfrp*$^{-/-}$ Zebrafish

We again utilized SD-OCT to image and measure the various metrics of *mfrp*$^{-/-}$; *mpeg1:*NTR-eYFP$^+$ eyes compared with the eyes of *mfrp*$^{+/-}$; *mpeg1:*NTR-eYFP$^+$ siblings with and without MTZ treatment (Fig. 4A). As in WT fish, MTZ treatment slowed overall growth in both *mfrp*$^{+/-}$ and *mfrp*$^{-/-}$ fish (Fig. 4B, body length). This effect was independent of *mpeg1:*NTR-eYFP expression (Supplementary Figs. S2A, S2B).

To control for the overall growth effect of MTZ treatment and possible genotype effects specific to *mfrp*, we MTZ treated *mfrp*$^{+/-}$, and *mfrp*$^{-/-}$ fish lacking the *mpeg1:*NTR-eYFP transgene and again imaged and measured the various eye and body metrics. We found that MTZ treatment affected axial length normalized to body length in these non-transgenic animals ($P = 0.0043$, 2-way analysis of variance

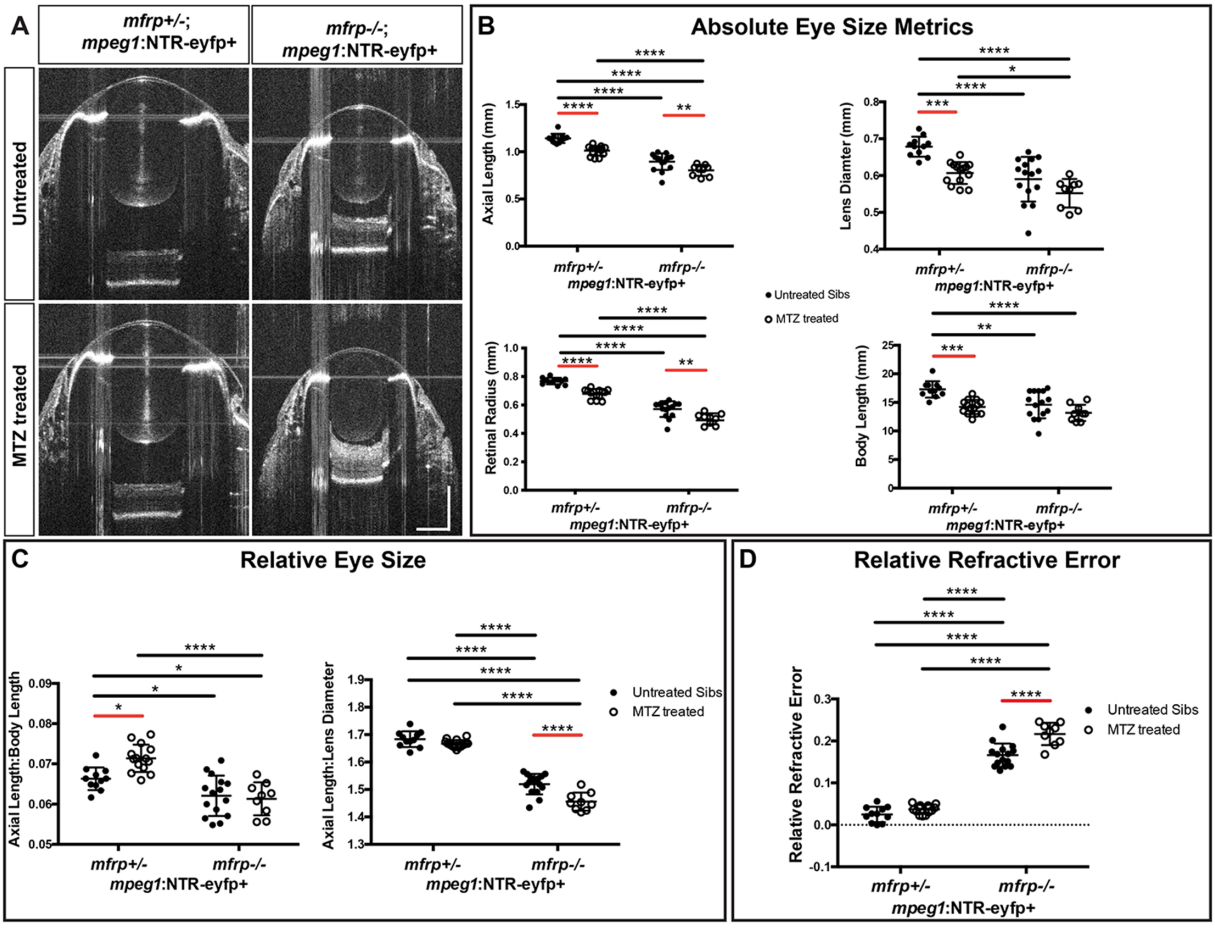

Figure 4. Macrophage ablation exacerbated hyperopia in *mfrp*$^{-/-}$ zebrafish. (**A**) Representative SD-OCT B-scans from the center of *mfrp*$^{+/-}$; *mpeg1:*NTR-eYFP$^+$ eyes and their *mfrp*$^{-/-}$; *mpeg1:*NTR-eYFP$^+$ siblings with or without MTZ treatment. (**B**) Eye size metrics of *mfrp*$^{+/-}$; *mpeg1:*NTR-eYFP$^+$ and *mfrp*$^{-/-}$; *mpeg1:*NTR-eYFP$^+$ fish with or without MTZ treatment. (**C**) Axial length normalized to body length and lens diameter. (**D**) Relative refractive error. Two-way ANOVA was used for statistical analysis. *P* values are shown from Tukey's multiple comparisons for post hoc analysis. *Error bars* represent standard deviation. *Red bars* indicate statistical significance due to MTZ treatment. $^*P < 0.05$, $^{**}P < 0.01$, $^{***}P < 0.001$, $^{****}P < 0.0001$. For *mfrp*$^{+/-}$ untreated, $n = 11$; for *mfrp*$^{+/-}$ MTZ treated, $n = 14$; for *mfrp*$^{-/-}$ untreated, $n = 15$; for *mfrp*$^{-/-}$ MTZ treated, $n = 9$.

Investigative Ophthalmology & Visual Science

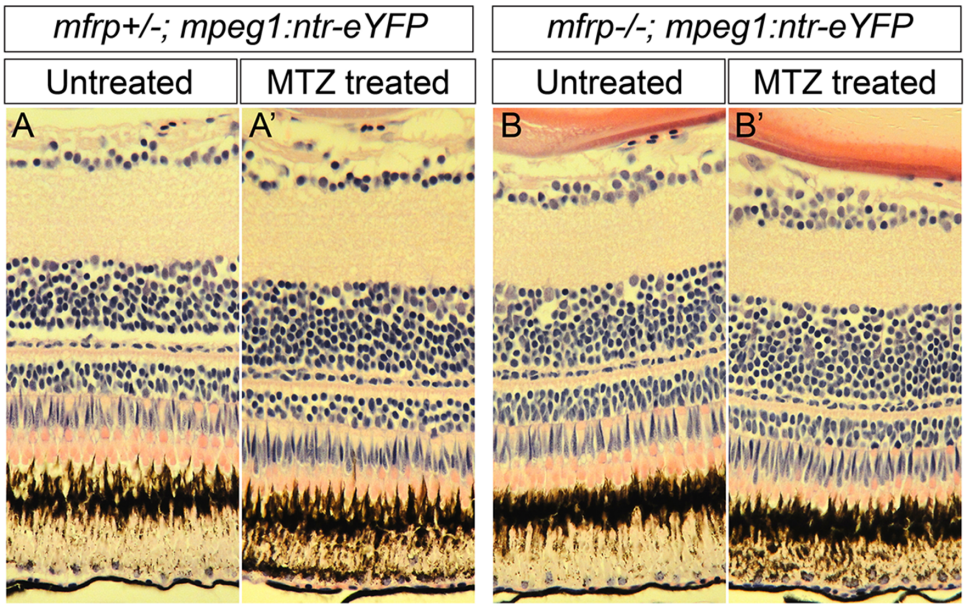

Figure 5. Macrophage ablation did not significantly alter retina morphology. (**A–B'**) Hematoxylin and eosin–stained paraffin histology of the central retina in *mfrp*$^{+/-}$; *mpeg1:*NTR-eYFP^{+} (**A**, **A'**) and *mfrp*$^{-/-}$; *mpeg1:*NTR-eYFP^{+} (**B**, **B'**) with and without MTZ treatment.

[ANOVA]) (Supplementary Fig. S2C). Although this might suggest a potential nonspecific effect of MTZ treatment on relative eye size, differences were not observed for axial length normalized to lens diameter in these non-transgenic control fish ($P = 0.3664$, 2-way ANOVA) (Supplementary Fig. S3C). Given that body length does not impact emmetropization, while lens diameter directly impacts this process, we concluded that MTZ treatment alone does not alter emmetropization in a nonspecific fashion. Further supporting this conclusion, relative refractive error was not significantly affected by MTZ treatment in these non-transgenic controls ($P = 0.2646$, 2-way ANOVA).

As expected, *mfrp*$^{-/-}$ fish had significantly reduced relative eye size compared with their *mfrp*$^{+/-}$ siblings when normalized to either body length or lens diameter ($P < 0.0001$, 2-way ANOVA) (Fig. 4C). Relative refractive error was also significantly increased in *mfrp*$^{-/-}$ fish compared with *mfrp*$^{+/-}$ siblings, as previously reported (Fig. 4D).[16] These results confirm that loss of *mfrp* leads to hyperopia in zebrafish and reveal that *mpeg*$^{+}$ cell ablation does not rescue this phenotype.

When we assessed the effect of macrophage ablation on relative eye size we found that MTZ treatment had significant effects (Fig. 4C, axial length to lens diameter; $P < 0.0001$, 2-way ANOVA). Post hoc analysis confirmed that *mfrp*$^{-/-}$; *mpeg1:*NTR-eYFP^{+} fish had a significantly decreased axial length normalized to lens diameter compared with their untreated *mfrp*$^{-/-}$; *mpeg1:*NTR-eYFP^{+} siblings (Fig. 4C). Nonspecific effects were not observed for axial length relative to lens diameter in animals that lacked the *mpeg1:*NTR-eYFP transgene ($P = 0.3664$, 2-way ANOVA) (Supplementary Fig. S2C), indicating that the change in relative eye size in *mfrp*$^{-/-}$ fish was specific to *mpeg1*$^{+}$ cell ablation. These effects were genotype specific, with *mfrp*$^{+/-}$; *mpeg1:*NTR-eYFP^{+} siblings showing no significant changes in axial length relative to lens diameter.

Finally, relative refractive error was also significantly affected by MTZ treatment in *mpeg:*NTR-eYFP–expressing fish ($P < 0.0001$, 2-way ANOVA) (Fig. 4D), but not in non-transgenic controls ($P = 0.2646$, 2-way ANOVA). Post hoc analysis confirmed a significant increase in relative refractive error in *mfrp*$^{-/-}$; *mpeg1:*NTR-eYFP^{+} fish compared with their untreated *mfrp*$^{-/-}$ siblings (Fig. 4D). Again, this was genotype specific, with *mfrp*$^{+/-}$; *mpeg1:*NTR-eYFP^{+} siblings showing no significant changes due to MTZ treatment. These results demonstrate that macrophage ablation significantly exacerbates the hyperopic phenotype of *mfrp* mutant zebrafish, indicating that the accumulation of macrophages seen in *mfrp*-related hyperopia may be recruited to ameliorate the microphthalmia.

Macrophage Ablation Did Not Significantly Alter Retina Morphology

As *mpeg1*$^{+}$ cell ablation affected relative eye size and refractive error, we sought to gain possible mechanistic insight into these changes by assessing overall eye and retinal morphology. We assessed the effects of macrophage ablation on overall retina morphology by histology. Hematoxylin and eosin–stained paraffin sections revealed normal retinal morphology following macrophage ablation (Figs. 5A–5B'). We did note that MTZ-treated eyes displayed more uniform and dispersed melanin throughout the cells of the RPE (Figs. 5A', 5B'). The rod outer segment layer also appeared shorter when compared with untreated siblings, possibly due to contraction of the myoid. These morphological changes are reminiscent of the retinomotor changes seen in dark adapted zebrafish.[26]

Neither Proliferation Nor Cell Death Underlay Exacerbated *mfrp*-Related Hyperopia After Macrophage Ablation

We hypothesized that the exacerbated changes in relative eye size seen in *mfrp* mutants could be due to altered cell

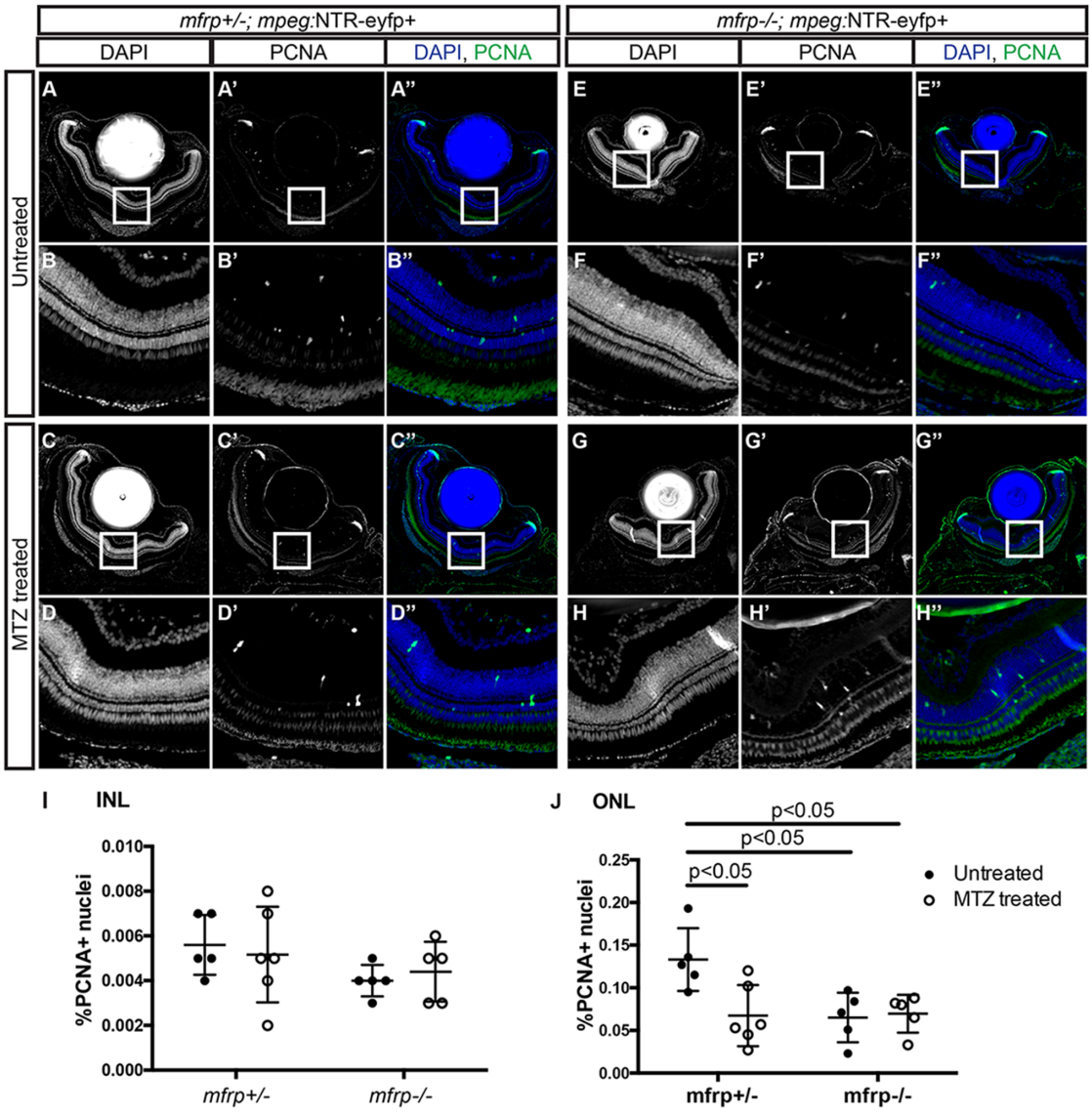

Figure 6. Proliferative effects of *mfrp* deletion and macrophage ablation. (**A–H**) Representative images of central retina sections from *mfrp*$^{+/-}$; *mpeg1:*NTR-eYFP^{+} and *mfrp*$^{-/-}$; *mpeg1:*NTR-eYFP^{+} MTZ treated and untreated fish. (**A–H**) Grayscale DAPI images at low magnification (**A**, **C**, **E**, **G**) and high magnification (**B**, **D**, **F**, **H**). (**A'–H'**) Grayscale PCNA images at low magnification (**A'**, **C'**, **E'**, **G'**) and high magnification (**B'**, **D'**, **F'**, **H'**). (**A"–H"**) Colorized merged images with DAPI in *blue* and PCNA in *green*; images are at low magnification (**A"**, **C"**, **E"**, **G"**) and high magnification (**B"**, **D"**, **F"**, **H"**). (**I–J**) Quantification of the percentage of PCNA^{+} nuclei in the inner (**I**) and outer (**J**) nuclear layer. *Error bars* represent standard deviations. Two-way ANOVA was used for statistical analysis for (**I**) and (**J**). *P* values are shown from Tukey's multiple comparisons for post hoc analysis. For *mfrp*$^{+/-}$ untreated, $n = 5$; for *mfrp*$^{+/-}$ MTZ treated, $n = 6$; for *mfrp*$^{-/-}$ untreated, $n = 5$; for *mfrp*$^{-/-}$ MTZ treated, $n = 5$.

proliferation and/or death. To assess changes in proliferation we performed immunohistochemistry for proliferative cell nuclear antigen (PCNA), along with DAPI to label nuclei. In *mfrp*$^{+/-}$; *mpeg1:*NTR-eYFP^{+} eyes, PCNA^{+} nuclei were found frequently within both the INL and ONL, as well as in the ciliary marginal zone. In comparison, *mfrp*$^{-/-}$; *mpeg1:*NTR-eYFP^{+} fish had PCNA^{+} cell frequency within the INL similar to that of their heterozygous siblings but significantly decreased frequency of PCNA^{+} nuclei in the ONL (Figs. 6A–6B", 6E–6F", 6I, 6J). No changes in the ciliary marginal zone were noted under any condition. MTZ treatment did significantly decrease the percentage of PCNA^{+} nuclei in the ONL of *mfrp*$^{+/-}$; *mpeg1:*NTR-eYFP^{+} fish compared with their untreated siblings (Figs. 6C–6D", 6J). PCNA analysis also revealed that *mfrp*$^{-/-}$ had reduced numbers of proliferative cells in the ONL, although, MTZ treatment on *mfrp*$^{-/-}$; *mpeg1:*NTR-eYFP^{+} animals did not exacerbate this effect (Figs. 6G–6H", 6J).

As an alternative to changes in cell proliferation, cell death caused by *mpeg*$^{+}$ cell ablation could lead to the decrease in relative eye size observed in *mfrp* mutants. To assess cell death, we performed terminal deoxynucleotidyl transferase dUTP nick end labeling (TUNEL). We found little or no TUNEL-positive cells regardless of genotype or treatment condition, suggesting that apoptosis did not cause the altered phenotype in *mfrp* mutant eyes (Supplementary Figs. S3A–S3C"'). Consistent with this result, DAPI staining did not reveal pyknotic nuclei for any genotype.

Investigative Ophthalmology & Visual Science

These results demonstrate that, although macrophage ablation may affect a small number of proliferative cells in the retina, it does not affect apoptosis, and neither cellular process appears to underlie the exacerbated hyperopia measured in macrophage-ablated *mfrp*$^{-/-}$ fish.

Macrophage Ablation Alters Collagen Bundle Size

Past research suggests that scleral collagen synthesis, degradation, and crosslinking play important roles during emmetropization, and this balance is altered during myopia.[27,28] We hypothesized that collagen fibers in the sclera of *mfrp* mutants may be altered and contribute to their improper emmetropization. To test this, we imaged collagen fibers in the central posterior region of the scleral stroma by TEM (Supplementary Fig. S4). Of note, we saw no obvious shifts in sclera thickness in any condition. By measuring and plotting the frequency distribution of collagen fiber diameters in the posterior sclera, we observed that the posterior scleral tissue in untreated *mfrp*$^{-/-}$; *mpeg1:*NTR-eYFP^{+} fish appeared to contain a slightly wider distribution of collagen bundle sizes with a small increase in the proportion of collagen fibers with larger diameters compared with their untreated *mfrp*$^{+/-}$; *mpeg1:*NTR-eYFP^{+} siblings (Figs. 7A, 7B). MTZ treatment exacerbated these differences (Figs. 7C, 7D). When compared with their untreated siblings, MTZ-treated *mfrp*$^{+/-}$; *mpeg1:*NTR-eYFP^{+} fish displayed a clear shift in collagen bundle diameter, increasing the frequency of smaller collagen bundles and decreasing the frequency of larger bundles (Fig. 7E). These results suggest that macrophage ablation can affect scleral collagen bundle size. However, these changes in scleral collagen fibril diameter do not appear to directly underlie the exacerbated *mfrp*-related hyperopia following macrophage ablation, as we did not find significant changes in fibril diameter between the MTZ-treated *mfrp*$^{-/-}$; *mpeg1:*NTR-eYFP^{+} and their untreated *mfrp*$^{-/-}$; *mpeg1:*NTR-eYFP^{+} siblings.

Macrophage Ablation Altered Collagen Accessibility to a CHP

Recent improvement in the detection of collagenous proteins has come in the form of CHPs, which specifically hybridize to degraded or unfolded collagen chains.[29–31] The collagen triple helix structure is made of repeating glycine–X–Y repeats, where the X and the Y are most often proline and hydroxyproline. CHP contains a repeating glycine–proline–hydroxyproline amino acid triplet which gives it high binding propensity for unfolded collagen and little affinity for intact collagen. Fluorescent conjugates of these CHPs have been validated in various species, tissues, and pathologies.[30] To assess collagen accessibility in both untreated and MTZ-treated conditions, we used a Cy3-conjugated CHP to stain *mfrp*$^{+/-}$; *mpeg1:*NTR-eYFP^{+} and *mfrp*$^{-/-}$; *mpeg1:*NTR-eYFP^{+} paraffin sections and counterstained with DAPI for orientation (Figs. 8A–8C). We quantified the mean pixel intensity of the R-CHP stain across both the entirety of the sclera (Fig. 8D) and over regions of interest in the posterior sclera (Fig. 8E). In both the whole sclera analysis ($P = 0.001$) and the posterior sclera analysis ($P = 0.0204$), genotype had a significant effect on the mean pixel intensity (2-way ANOVA), with *mfrp*$^{-/-}$ eyes appearing to have slight decreases in R-CHP intensity. In the whole sclera analysis, MTZ treatment also had a significant effect on mean pixel intensity ($P = 0.022$, 2-way ANOVA). Applying post hoc statistical analysis, we found that *mfrp*$^{-/-}$; *mpeg1:*NTR-eYFP^{+} fish treated with MTZ exhibited significantly less R-CHP staining intensity than their untreated *mfrp*$^{-/-}$; *mpeg1:*NTR-eYFP^{+} siblings ($P = 0.0319$, Sidak's multiple comparison) (Fig. 8D). These results suggest that *mfrp*$^{-/-}$ fish have lower levels of denatured or unfolded collagens than their *mfrp*$^{+/-}$ siblings and that macrophage ablation exacerbates this difference. This change in collagen architecture might underlie the exacerbated hyperopia seen in *mfrp*$^{-/-}$ eyes after macrophage ablation.

Discussion

We found that depletion of macrophages exacerbated *mfrp*-related hyperopia in zebrafish. Additionally, we observed that, although macrophages affect the development of *mfrp*-related hyperopia, the absence of the *mpeg-1* population did not significantly alter WT emmetropization. We went on to investigate further how macrophage ablation might affect morphology and growth of retina and sclera, examining changes in retinal cell proliferation and changes in scleral collagen fibers.

We noted the nonspecific effects of MTZ treatment on the overall size of the fish and accounted for these changes in our analysis. MTZ could cause additional non-obvious effects. MTZ itself is an antibiotic that was originally used for the treatment of trichomoniasis,[32,33] and it continues to be used to combat anaerobic infections.[34] Daily antibiotic washes on zebrafish likely have a profound effect on the microbiome of the fish and could result in unintended effects. Metronidazole has also been shown to affect circadian rhythm, increasing the expression of core clock genes in the skeletal muscle of germ-free mice.[35] However, this MTZ-based ablation technique has been used to study circadian rhythms of visual sensitivity in zebrafish, and no alterations to circadian rhythm were reported in non-transgenic MTZ treated fish.[36] To control for potential nonspecific effects of MTZ, all non-transgenic control groups were treated exactly as the transgene-expressing experimental groups and underwent the same MTZ treatment regimen.

Notably macrophage ablation only affected emmetropization in the context of *mfrp*-related hyperopia and showed no effect in WT conditions. This finding led us to hypothesize that macrophages are recruited in *mfrp*$^{-/-}$ eyes to help preserve proper refractive state. How the loss of Mfrp, a protein expressed primarily in the RPE and ciliary epithelium, results in macrophage recruitment remains an open question. Recently, zebrafish RPE were shown to express leukocyte recruitment factors among other immune-related genes following genetic ablation.[37] Leach et al.[37] went on to show that the macrophage and microglia cells that are recruited are also required for proper RPE regeneration, demonstrating that macrophages play a crucial role in the health of the RPE following injury. This raises the possibility that the RPE of *mfrp*$^{-/-}$ zebrafish exists in an injury-like state leading to recruitment of macrophages. Interestingly, macrophage depletion in mice via colony stimulating factor 1 receptor inhibition was associated with loss of proper RPE structure, which could be rescued following repopulation of macrophages.[38] Studies such as these highlight crucial signaling between these two populations of cells in RPE maintenance and regeneration. Our data demonstrate that this crosstalk between RPE and macrophages also affects pathological hyperopia in the context of loss of *mfrp*.

Investigative Ophthalmology & Visual Science

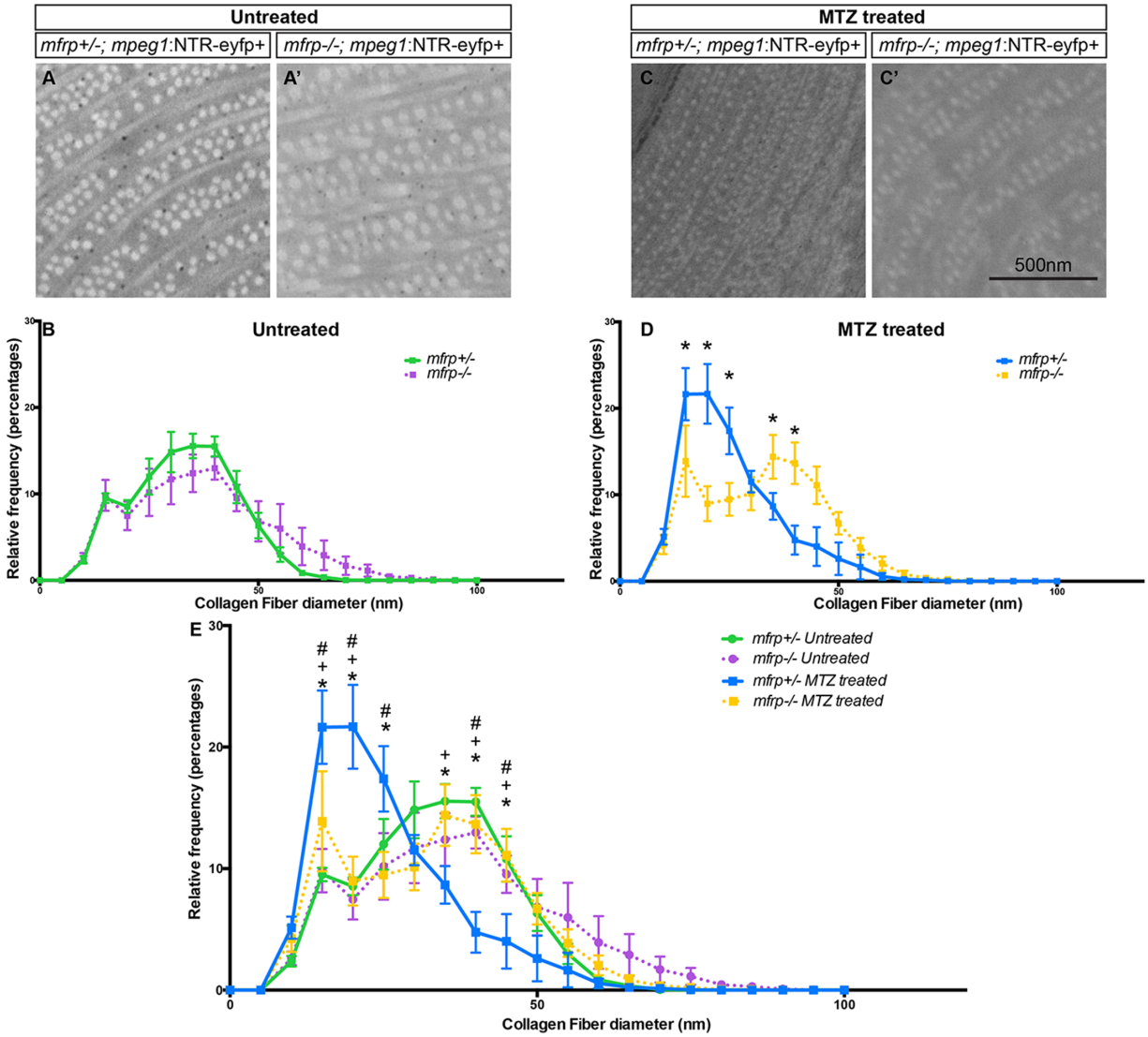

Figure 7. Collagen fibril diameter in *mfrp*$^{+/-}$ and *mfrp*$^{-/-}$ sclera with and without macrophage ablation. Representative examples of collagen fibrils in the central posterior sclera of *mfrp*$^{+/-}$; *mpeg1:*NTR-eYFP^{+} (**A**) and *mfrp*$^{-/-}$; *mpeg1:*NTR-eYFP^{+} (**A'**) untreated fish. (**B**) Frequency distribution of collagen fiber diameter with *y*-axis = relative frequency as a percentage and *x*-axis = collagen fiber diameter in 5-nm bins. *mfrp*$^{+/-}$ is indicated by a *green line*, *mfrp*$^{-/-}$ by a *purple line*. For *mfrp*$^{+/-}$, $n = 3$; for *mfrp*$^{-/-}$, $n = 4$. (**C**) Representative examples of collagen fibrils in the central posterior sclera of *mfrp*$^{+/-}$; *mpeg1:*NTR-eYFP^{+} (**C**) and *mfrp*$^{-/-}$; *mpeg1:*NTR-eYFP^{+} (**C'**) MTZ treated fish. (**D**) Frequency distribution of collagen fiber diameter with *y*-axis = relative frequency as a percentage and *x*-axis = collagen fiber diameter in 5-nm bins. *mfrp*$^{+/-}$ is represented by a *blue line*, *mfrp*$^{-/-}$ by a *yellow line*. For *mfrp*$^{+/-}$, $n = 5$; for *mfrp*$^{-/-}$, $n = 5$. Multiple *t*-tests were used for statistical analysis. *$P < 0.001$. (**E**) Combined graph of (**B**) and (**D**). *Errors bars* represent standard deviations throughout figure. Two-way ANOVA with Tukey's multiple-comparisons were used for statistical analysis. An asterisk (*) denotes a significant difference between *mfrp*$^{+/-}$ MTZ treated and *mfrp*$^{-/-}$ MTZ treated; a plus sign (+) denotes a significant difference between *mfrp*$^{+/-}$ MTZ treated and *mfrp*$^{+/-}$ untreated; and the pound symbol (#) denotes a significant difference between *mfrp*$^{+/-}$ MTZ treated and *mfrp*$^{-/-}$ untreated. $P < 0.05$ for all significant differences in (**E**).

Our ablation technique is limited to the cells expressing the *mpeg1:*NTR-eYFP transgene. In that context, this broad macrophage population is efficiently ablated by the action of the transgene. Still, 4C4^{+} macrophages remained following MTZ treatment, suggesting that non-*mpeg*$^{+}$ macrophages persist. Likewise, our histological analysis demonstrated that Lcp1^{+} macrophages also remained, although at reduced numbers. These findings highlight the heterogeneity of the population of monocyte-like cells in the retina, whether macrophage or microglia. It is clear that the *mpeg1:*NTR-eYFP transgene, although marking a broad population of macrophages, does not express in all retinal monocytes. Notably, both *mpeg1* positive and negative macrophages were elevated in the *mfrp* mutant retina. Future work investigating the importance of macrophage subtypes could prove useful for identifying their possible roles in emmetropization and potential additional effects on *mfrp* mutant pathogenesis. It seems likely that either the loss of Mfrp or the condition of hyperopia alters the state of macrophages in the retina or the recruitment of a separate subpopulation.

Finally, we found modulation of the collagen architecture following macrophage ablation. Recent work suggests that collagen bundle size is dynamically regulated during emmetropization, and these alterations in size can change

Investigative Ophthalmology & Visual Science

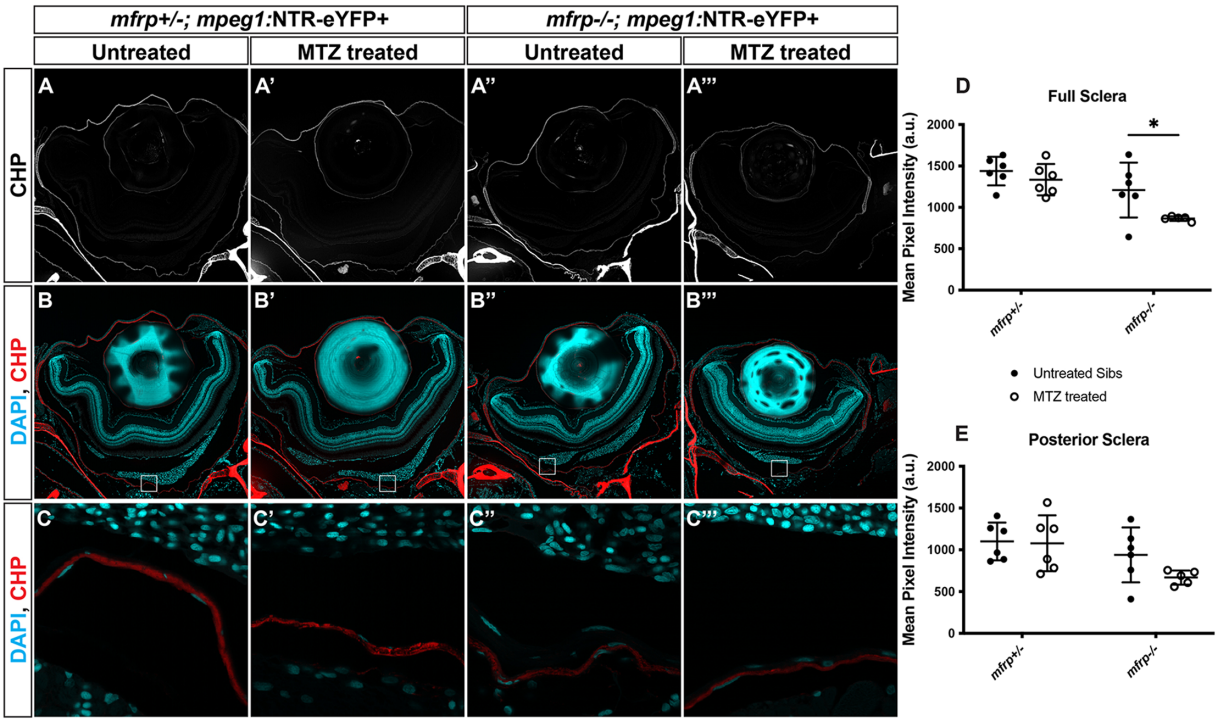

Figure 8. Macrophage ablation alters scleral accessibility to a collagen hybridizing peptide. (**A–C**) Representative images of central retina sections from *mfrp*$^{+/-}$; *mpeg1:*NTR-eYFP^{+} and *mfrp*$^{-/-}$; *mpeg1:*NTR-eYFP^{+} MTZ treated and untreated fish. (**A–A'''**) Grayscale CHP images. (**B–B'''**) Colorized and merged images with DAPI in *cyan* and CHP in *red*. (**C–C'''**) High-magnification images of regions of interest in the posterior sclera as indicated by *white outlines* in (**B**) to (**B'''**). (**D**, **E**) Quantification of the mean pixel intensity of the CHP staining across full sclera (**D**) and at central posterior sclera (**E**). For whole sclera (**D**), both genotype ($P = 0.001$) and MTZ treatment ($P = 0.022$) had a significant effects. In the posterior sclera (**E**) only genotype ($P = 0.0204$) had a significant effect. Two-way ANOVA was used for statistical analysis. *P* values are shown from Sidak's multiple comparisons for post hoc analysis. *Error bars* represent standard deviations. *$P < 0.05$. For *mfrp*$^{+/-}$ untreated, $n = 6$; for *mfrp*$^{+/-}$ MTZ treated, $n = 6$; for *mfrp*$^{-/-}$ untreated, $n = 6$; for *mfrp*$^{-/-}$ MTZ treated, $n = 5$.

their mechanical properties.[27] Recently, alterations in scleral collagen dynamics have been partially attributed to an increased presence of scleral macrophages in a visual form-deprived mouse model of myopia.[28] These investigators reported that macrophages appeared to be recruited to the sclera of form-deprived myopic mice by increased scleral expression of C-C motif chemokine ligand-2. The authors suggested that, upon recruitment, the macrophages are then partially responsible for the secretion of matrix metalloproteinase-2 in the sclera, resulting in extracellular matrix remodeling that contributes to the development of myopia. One possible hypothesis that stems from these data is that, as the retina grows, it exerts force on the sclera, and collagen remodeling alters scleral compliance, allowing axial elongation of the eye. In the case of *mfrp* mutant eyes, increased collagen bundle diameter may result in increased tensile stiffness of the sclera and prevent proper axial elongation. Indeed, we observed an upward trend in the percentage of collagen fibrils with larger diameter in *mfrp*$^{-/-}$ sclera when compared with their *mfrp*$^{+/-}$ siblings. In further support of these ideas, retinal folds are observed in *mfrp*$^{-/-}$ eyes.[16] Perhaps the retina itself continues to expand while the sclera cannot, and this forces the retina to fold in on itself. This is relevant to the foveoschisis seen in some patients with *MFRP*-related microphthalmia. Furthermore, MTZ treatment resulted in a clear shift of collagen fibril diameter distribution in *mfrp*$^{+/-}$; *mpeg1:NTR-eYFP*$^{+}$ fish, suggesting that the presence of macrophages can affect collagen fibril size. Supporting a direct role for macrophages, it has been reported that macrophages have the ability to directly secrete collagen in the context of scar formation after cardiac injury in zebrafish.[39] Further work is required to define the precise relationship between collagen fibril size and emmetropia, as it currently remains unclear if an alteration to scleral collagen in *mfrp* mutants is an underlying cause of improper refractive state or simply a response to that state.

Our data suggest that, although the presence or absence of macrophages can result in altered collagen fibril diameter, alteration alone is not sufficient to modulate axial length and affect emmetropization. To further examine the collagen architecture of the sclera we utilized a fluorescently conjugated CHP to assess collagen accessibility. Based on the significant effects of both genotype and MTZ treatment in this assay, we suggest that macrophage ablation resulted in a more rigid collagen extracellular matrix in *mfrp*$^{-/-}$ sclera. Less unfolded or denatured collagens may result in a less compliant sclera that is ultimately less amenable to axial elongation. We hypothesize that these alterations to collagen dynamics partially underlie the exacerbation of *mfrp*-related hyperopia we found following macrophage ablation.

To conclude, the most significant finding in this study is the role of the *mpeg1*$^{+}$ cell population in pathologic hyperopia, but not for wild-type emmetropization. To date, very little is known regarding the function of ocular macrophages in either normal or aberrant emmetropization. Our results therefore mark an initial understanding for the role of

Investigative Ophthalmology & Visual Science

macrophages in pathologic hyperopia and, more specifically, *mfrp*-related hyperopia in zebrafish.

Acknowledgments

The authors thank David Parichy (University of Virginia, Charlottesville) for sharing the *mpeg1*:NTR-eyfp transgenic line, Clive Wells (Director of the MCW Electron Microscopy core) for assistance with electron microscopy, and Pat Cliff and Erin Bentley for providing zebrafish husbandry.

Supported by a grant from the National Eye Institute, National Institutes of Health (R01EY29267). This investigation was conducted in a facility constructed with support from the Research Facilities Improvement Program (Grant C06RR016511) from the National Center for Research Resources, National Institutes of Health.

Disclosure: **Z.J. Brandt**, None; **R.F. Collery**, None; **J.C. Besharse**, None; **B.A. Link**, None

References

1. Bacci GM, Bargiacchi S, Fortunato P, et al. Novel mutations in *MFRP* and *PRSS56* are associated with posterior microphthalmos. *Ophthalmic Genet.* 2020;41:49–56.
2. Almoallem B, Arno G, De Zaeytijd J, et al. The majority of autosomal recessive nanophthalmos and posterior microphthalmia can be attributed to biallelic sequence and structural variants in MFRP and PRSS56. *Sci Rep.* 2020;10:1289.
3. Siggs OM, Souzeau E, Breen J, et al. Autosomal dominant nanophthalmos and high hyperopia associated with a C-terminal frameshift variant in *MYRF*. *Mol Vis.* 2019;25:527–534.
4. Lang E, Koller S, Atac D, et al. Genotype-phenotype spectrum in isolated and syndromic nanophthalmos. *Acta Ophthalmol.* 2021;99:e594–e607.
5. Crespí J, Buil JA, Bassaganyas F, et al. A novel mutation confirms MFRP as the gene causing the syndrome of nanophthalmos-renititis pigmentosa-foveoschisis-optic disk drusen. *Am J Ophthalmol.* 2008;146:323–328.e1.
6. Guo C, Zhao Z, Chen D, et al. Detection of clinically relevant genetic variants in Chinese patients with nanophthalmos by trio-based whole-genome sequencing study. *Invest Ophthalmol Vis Sci.* 2019;60:2904–2913.
7. Katoh M. Molecular cloning and characterization of MFRP, a novel gene encoding a membrane-type Frizzled-related protein. *Biochem Biophys Res Commun.* 2001;282:116–123.
8. Matsushita I, Kondo H, Tawara A. Novel compound heterozygous mutations in the MFRP gene in a Japanese patient with posterior microphthalmos. *Jpn J Ophthalmol.* 2012;56:396–400.
9. Sundin OH, Leppert GS, Silva ED, et al. Extreme hyperopia is the result of null mutations in MFRP, which encodes a Frizzled-related protein. *Proc Natl Acad Sci USA.* 2005;102:9553–9558.
10. Wasmann RA, Klein Wassink-Ruiter JS, Sundin OH, Morales E, Verheij JBGM, Pott JWR. Novel membrane frizzled-related protein gene mutation as cause of posterior microphthalmia resulting in high hyperopia with macular folds. *Acta Ophthalmol.* 2014;92:276–281.
11. Zenteno JC, Buentello-Volante B, Quiroz-González MA, Quiroz-Reyes MA. Compound heterozygosity for a novel and a recurrent MFRP gene mutation in a family with the nanophthalmos-retinitis pigmentosa complex. *Mol Vis.* 2009;15:1794–1798.
12. Fogerty J, Besharse JC. 174delG mutation in mouse MFRP causes photoreceptor degeneration and RPE atrophy. *Invest Ophthalmol Vis Sci.* 2011;52:7256–7266.
13. Won J, Smith RS, Peachey NS, et al. Membrane frizzled related protein is necessary for the normal development and maintenance of photoreceptor outer segments. *Vis Neurosci.* 2008;25:563–574.
14. Krebs MP, Hicks W, Nishina PM. Mfrp regulates ocular growth in mice and interacts with Prss56. *Invest Ophthalmol Vis Sci.* 2016;57:3609.
15. Velez G, Tsang SH, Tsai Y-T, et al. Gene therapy restores Mfrp and corrects axial eye length. *Sci Rep.* 2017;7:16151.
16. Collery RF, Volberding PJ, Bostrom JR, Link BA, Besharse JC. Loss of zebrafish Mfrp causes nanophthalmia, hyperopia, and accumulation of subretinal macrophages. *Invest Ophthalmol Vis Sci.* 2016;57:6805–6814.
17. Fogerty J, Besharse JC. Subretinal infiltration of monocyte derived cells and complement misregulation in mice with AMD-like pathology. *Adv Exp Med Biol.* 2014;801:355–363.
18. Zenteno JC, Buentello-Volante B, Quiroz-González MA, Quiroz-Reyes MA. Compound heterozygosity for a novel and a recurrent MFRP gene mutation in a family with the nanophthalmos-retinitis pigmentosa complex. *Mol Vis.* 2009;15:1794–1798.
19. Collery RF, Veth KN, Dubis AM, Carroll J, Link BA. Rapid, accurate, and non-invasive measurement of zebrafish axial length and other eye dimensions using SD-OCT allows longitudinal analysis of myopia and emmetropization. *PLoS One.* 2014;9:e110699.
20. Ellett F, Pase L, Hayman JW, Andrianopoulos A, Lieschke GJ. mpeg1 promoter transgenes direct macrophage-lineage expression in zebrafish. *Blood.* 2011;117:e49–e56.
21. Eom DS, Parichy DM. A macrophage relay for long distance signaling during post-embryonic tissue remodeling. *Science.* 2017;355:1317–1320.
22. Petrie TA, Strand NS, Tsung-Yang C, Rabinowitz JS, Moon RT. Macrophages modulate adult zebrafish tail fin regeneration. *Development.* 2014;141:2581–2591.
23. Curado S, Stainier DYR, Anderson RM. Nitroreductase-mediated cell/tissue ablation in zebrafish: a spatially and temporally controlled ablation method with applications in developmental and regeneration studies. *Nat Protoc.* 2008;3:948–954.
24. Becker T, Becker CG. Regenerating descending axons preferentially reroute to the gray matter in the presence of a general macrophage/microglial reaction caudal to a spinal transection in adult zebrafish. *J Comp Neurol.* 2001;433:131–147.
25. Redd MJ, Kelly G, Dunn G, Way M, Martin P. Imaging macrophage chemotaxis in vivo: studies of microtubule function in zebrafish wound inflammation. *Cell Motil.* 2006;63:415–422.
26. Hodel C, Neuhauss SCF, Biehlmaier O. Time course and development of light adaptation processes in the outer zebrafish retina. *Anat Rec A Discov Mol Cell Evol Biol.* 2006;288:653–662.
27. Ouyang X, Han Y, Xie Y, et al. The collagen metabolism affects the scleral mechanical properties in the different processes of scleral remodeling. *Biomed Pharmacother.* 2019;118:109294.
28. Zhao F, Wu H, Reinach PS, et al. Up-regulation of matrix metalloproteinase-2 by scleral monocyte-derived macrophages contributes to myopia development. *Am J Pathol.* 2020;190:1888–1908.
29. Li Y, Ho D, Meng H, et al. Direct detection of collagenous proteins by fluorescently labeled collagen mimetic peptides. *Bioconjug Chem.* 2013;24:9–16.
30. Hwang J, Huang Y, Burwell TJ, et al. In situ imaging of tissue remodeling with collagen hybridizing peptides. *ACS Nano.* 2017;11:9825–9835.

Investigative Ophthalmology & Visual Science

31. Zitnay JL, Li Y, Qin Z, et al. Molecular level detection and localization of mechanical damage in collagen enabled by collagen hybridizing peptides. *Nat Commun*. 2017;8:14913.
32. Nicol CS, Barrow J, Redmond A. Flagyl (8823 R.P.) in the treatment of trichomoniasis. *Sex Transm Infect*. 1960;36:152–153.
33. Watt L, Jennison RF. Clinical evaluation of metronidazole. *Br Med J*. 1960;2:902–905.
34. Löfmark S, Edlund C, Nord CE. Metronidazole is still the drug of choice for treatment of anaerobic infections. *Clin Infect Dis*. 2010;50:S16–S23.
35. Manickam R, Oh HYP, Tan CK, Paramalingam E, Wahli W. Metronidazole causes skeletal muscle atrophy and modulates muscle chronometabolism. *Int J Mol Sci*. 2018;19:2418.
36. Li X, Montgomery J, Cheng W, Noh JH, Hyde DR, Li L. Pineal photoreceptor cells are required for maintaining the circadian rhythms of behavioral visual sensitivity in zebrafish. *PLoS One*. 2012;7:e40508.
37. Leach LL, Hanovice NJ, George SM, Gabriel AE, Gross JM. The immune response is a critical regulator of zebrafish retinal pigment epithelium regeneration. *Proc Natl Acad Sci USA*. 2021;118:e2017198118.
38. Yang X, Zhao L, Campos MM, et al. CSF1R blockade induces macrophage ablation and results in mouse choroidal vascular atrophy and RPE disorganization. *eLife*. 2020;9:e55564.
39. Simões FC, Cahill TJ, Kenyon A, et al. Macrophages directly contribute collagen to scar formation during zebrafish heart regeneration and mouse heart repair. *Nat Commun*. 2020;11:600.

Investigative Ophthalmology & Visual Science